Published in final edited form as:
Biochemistry. 2012 November 27; 51(47): 9547–9559. doi:10.1021/bi301278t.

The Ω-loop lid domain of phosphoenolpyruvate carboxykinase is essential for catalytic function

Troy A. Johnson[1,†] and **Todd Holyoak**[1,2]

[1]Department of Biochemistry and Molecular Biology. The University of Kansas Medical Center, Kansas City, KS 66160

[2]Department of Biology, University of Waterloo, Waterloo ON N2L 3G1

Abstract

Phosphoenolpyruvate carboxykinase (PEPCK) is an essential metabolic enzyme operating in the gluconeogenesis and glyceroneogenesis pathways. Recent studies have demonstrated that the enzyme contains a mobile active site lid domain that transitions between an open/disorded conformation to a closed/ordered conformation as the enzyme progresses through the catalytic cycle. The understanding of how this mobile domain functions in catalysis is incomplete. Previous studies show that the closure of the lid domain stabilizes the reaction intermediate and protects the reactive intermediate from spurious protonation and thus contributes to the fidelity of the enzyme. In order to more fully investigate the roles of the lid domain in PEPCK function we created three mutations that replaced the 11-residue lid domain with one, two or three glycine residues. Kinetic analysis of the mutant enzymes demonstrates that none of the enzyme constructs exhibit any measurable kinetic activity resulting in a decrease in the catalytic parameters by at least 10^6. Structural characterization of the mutants in complexes representing the catalytic cycle suggest that the inactivity is due to a role for the lid domain in the formation of the fully closed state of the enzyme that is required for catalytic function. In the absence of the lid domain, the enzyme is unable to achieve the fully closed state and is rendered inactive despite possessing all of the residues and substrates required for catalytic function. This work demonstrates how enzyme catalytic function can be abolished through the alteration of conformational equilibria despite all elements required for chemical conversion of substrates to products remaining intact.

The molecular processes an enzyme utilizes to bind substrate, cross the transition state barrier, and release product has been an area of active research for decades. It is well understood that enzymes are not rigid in solution, rather they are flexible molecules capable of sampling multiple conformations to adapt a catalytically active form (1). These molecular motions can vary in amplitude, rate and the size of the mobile element covering changes as diverse as vibrational modes of individual bonds, side chain rotameric shifts, and whole domain rearrangements. While biophysical characterization of enzyme structures frequently demonstrates alterations in the positions of secondary structural elements of enzymes (α-helices, β-strands) as a function of ligation state, non-regular secondary structure elements (loops and turns) due to their inherent conformational flexibility often play a vital role in enzyme function (2, 3). One non-regular secondary structure that has been described in

Corresponding Author Todd Holyoak, Department of Biology, University of Waterloo, Waterloo ON N2L 3G1, Telephone 519-888-4567 x31565; todd.holyoak@uwaterloo.ca.
[†]Present address: Baylor College of Medicine, Houston TX

Coordinates and structure factors have been deposited in the RCSB protein databank (http://www.rcsb.org/pdb) under the accession codes 4GMM, 4GMW, 4GMU, 4GMZ, 4GNL, 4GNM, 4GNO, 4GNP, and 4GNQ.

No competing financial interests have been declared.

numerous enzymes is the omega-loop Ω-loop) (4-8). An Ω-loop is an ~10-20 amino acid loop characterized by its resemblance to the Greek letter omega due to a very narrow end-to-end distance (typically 3-5 Å, Figure 1) (2). This type of loop is predominantly found on the protein surface and has been observed to undergo displacements of up to 10 Å at the tip (9). While Ω-loops are prevalent in enzyme structure, there is no sequence consensus, simply the requirement for a close end-to-end distance at the points of exit and reentry to the body of the protein. Where it has been characterized the Ω-loop has been shown to function as a singular hinged domain and that the flexibility limits on the hinge are vitally important to the ability of the loop to alternate between two discrete orientations (open and closed) rather than functioning as a conformationally disordered structural element (10). Typically this equilibrium between open/closed states is altered by the presence/absence of substrates/ products or more generally enzyme ligation states (9, 11, 12). One enzyme that has been structurally characterized and found to have a functionally important Ω-loop is phosphoenolpyruvate carboxykinase (PEPCK)[1] (4, 11, 13, 14).

In humans, PEPCK exists as two isoforms. One isoform is located in the cytosol (cPEPCK) while the other resides in the mitochondria (mPEPCK). While the metabolic role of mPEPCK is poorly understood, cytosolic PEPCK (cPEPCK) is typically assigned a role in the gluconeogenic and glyceroneogenic pathways. However, recent work suggests that cPEPCK should be considered to function as a more general cataplerotic enzyme (16).

The reaction catalyzed by PEPCK involves the decarboxylation and phosphorylation of oxaloacetate (OAA) to form phosphoenolpyruvate (PEP), utilizing a nucleotide triphosphate as the phosphoryl donor (Scheme 1). The reaction is freely reversible *in vitro*, but is thought to operate primarily in the direction of PEP synthesis *in vivo*. PEPCK requires two divalent cations for enzymatic activity. In the GTP-dependent isoforms found in humans and other vertebrates, one cation (M1), preferably Mn^{2+}, associates with the enzyme in the absence of substrates while the additional metal ion (M2), typically Mg^{2+} binds as the metal-nucleotide substrate (17-19). GTP-dependent PEPCK has been extensively characterized biochemically and, more recently, structurally (reviewed in (20)). Examination of the structural data on the GTP-dependent PEPCKs indicates that the enzyme is composed of an N-terminal lobe (residues 1-259) and a C-terminal lobe (residues 260-622) with the active site lying in the cleft between the two lobes (Figure 2). The C-terminal lobe can be further subdivided into two domains, the nucleotide binding domain (residues 260-325 and 426-622) which has limited homology to other nucleotide binding proteins and enzymes, and the PEPCK-specific domain (residues 326-425), so named do to structural alignments suggesting that this domain is present only within the PEPCK family (Figure 2). The structural data also reveal several previously unappreciated features of PEPCK. Specifically, inspection of the structural data reveals several mobile loops whose conformation and/or mobility is impacted by the ligation state of the enzyme along the reaction coordinate. The most noticeable elements are the R-loop (residues 85-92), the P-loop (residues 284-292), and the Ω-loop lid (residues 464-474) (Figure 1)(20). Further, similar to what is observed in the ATP-dependent isoform from *E.coli* (21) a global motion that involves the opening and closing of the N- and C-terminal lobes of the enzyme is also observed (20). Due to their location at the active site, the R-loop and the P-loop are thought to be involved directly in substrate binding and catalysis. The Ω-loop and the movement of the N- and C-terminal lobes transition between open and closed conformations; an equilibrium that is influenced by the nature of

[1]**ABBREVIATIONS** ADP, adenosine-5′-diphosphate; ASU, asymmetric unit; βME, 2-mercaptoethanol; ßSP, 3-sulfopyruvate; cPEPCK, cytosolic phosphoenolpyruvate carboxykinase; DTT, dithiothreitol; GDP, guanosine-5′-diphosphate; GTP, guanosine-5′-triphosphate; IDP, inosine-5′-diphosphate; ITP, inosine-5′-triphosphate; LDH, lactate dehydrogenase; MDH, malate dehydrogenase; OAA, oxaloacetic acid; PEG, polyethylene glycol; PEP, phosphoenolpyruvate; PEPCK, phosphoenolpyruvate carboxykinase; PGA, 2-phosphoglycolate; PK, pyruvate kinase; RMSD, root-mean-square-deviation; SUMO, small ubiquitin-like modifier; TCEP, tris(2-carboxyethyl)phosphine.

the substrates/products bound (20). The P-loop movement serves two purposes. First, its closure/ordering upon nucleotide binding removes a potential steric clash between T465 on the Ω-loop and A287 on the P-loop allowing the Ω-loop lid to sample its closed conformation. Secondly, typical to other kinases it cradles the β- and γ-phosphates of GDP/GTP and positions the invariant P-loop lysine (K290 in cPEPCK) in a position to activate the phosphate leaving group allowing for direct inline phosphoryl transfer (20). Once GTP is positioned for phosphoryl transfer and OAA is bound, the structural data suggest that the chemical reaction is initiated by the movement of the N- and C-terminal lobes toward one another via a 'clam like' closure of the two domains. The lobe closure effectively reduces the size of the active site, and causes the nucleotide and its associated cation to shift on the order of 1-2Å toward OAA and the M1 Mn^{2+} ion. Coincident with lobe closure, the Ω-loop is observed to adapt the closed conformation stabilized primarily through interactions between E469 and H470 in the ω-loop and E89 on the R-loop (13). It is only upon lobe and ω-loop closure that all substrates are correctly positioned for catalysis. Consistent with this proposed mechanism, it has been demonstrated that a disruption in the ability of the ω-loop to adapt its closed conformation results in decreased catalytic efficiency and a loss in catalytic fidelity (14).

An ω-loop secondary structure, which undergoes an open/closed transition, has been reported for other enzymes such as: triosephosphate isomerase, glutathione synthetase, and ribulose-1,5-bisphosphate carboxylase/oxygenase (6-9). Biochemical and crystallographic studies of these enzymes resulted in widely differing roles for the ω-loop domain being proposed. Based upon study of these aforementioned enzymes, an ω-loop can sequester and protect reaction intermediates, recruit charged groups to the active site, aid in correctly positioning substrates and side chains, stabilize specific enzyme conformations and alter the active site environment to facilitate the required chemistry (3, 7-9, 12). Based on the available data on PEPCK, the role of the ω-loop is to aid in correctly positioning substrates in the active site, and to sequester and protect the reaction intermediate (14). To further interrogate and probe for additional roles of the ω-loop lid domain of PEPCK, three lid deletion mutants were created (Figure 3). Each construct removed the entire lid domain (residues 464-474) and replaced the 11 excised residues with one (Ld_1g), two (Ld_2g), or three (Ld_3g) glycine residues. Kinetic characterization of these mutant enzymes demonstrates that the ω-loop is absolutely required for enzymatic activity despite the loop contributing no residues to the catalytic mechanism. Further, the structural data provide evidence as to the mechanism for this essential requirement, namely that the ω-loop acts to facilitate the ability of the enzyme to adapt the catalytically necessary fully closed conformation of the N- and C-terminal lobes and to act as a thermodynamic latch stabilizing that same conformation.

EXPERIMENTAL PROCEDURES

Materials

The nucleotides (GDP, GTP, IDP, ITP, and ADP) were purchased from Sigma. PEP and NADH were from Chem-Impex. DTT and TCEP were from Gold Bio-Tech. HEPES buffer was from Research Organics. Oxalic acid was from Fluka. 3-sulfopyruvate (βSP) was synthesized and purified as previously described (22). Ni-NTA resin was purchased from Qiagen. HiQ, P6DG, and Chelex resins were from Bio-Rad. All other materials were of the highest grade commercially available.

Enzymes

The coupling enzymes used in the kinetic assays for PEPCK, malate dehydrogenase (Calzyme), lactate dehydrogenase (Calzyme) and pyruvate kinase (Roche) were used as provided by the supplier.

The plasmid expressing His_6-SUMO protease was a gift from Dr. Christopher Lima (Sloan Kettering Institute). The protease was expressed and purified by the following procedure. A 5 mL overnight culture of BL-21(DE3) *E. coli* cells containing the His_6-SUMO plasmid were grown at 37 °C, 225 rpm in LB media supplemented with 50 μg/mL kanamycin. The cells from this culture were pelleted by centrifugation at 6000 rpm. The resultant cell pellet was resuspended and 5 mL was used to inoculate 1 L of fresh LB-kanamycin medium in a 2.8 L-baffled flask. This culture was grown at 37 °C until the OD_{600} reached 2.0. The temperature was lowered to 30 °C and after 15 min the expression of the protease was induced by the addition of IPTG at a final concentration of 0.75 mM. The cells were grown under these conditions for an additional four hours and then harvested by centrifugation at 6000rpm for 15 min and subsequently stored at −80 °C. The frozen pellet was resuspended in 20 mM Tris-HCl, pH 8.0, 350 mM NaCl, 1mM ßME and 20 mM imidazole and lysed by two passages through a French pressure cell. The cell debris was pelleted by centrifugation at 9000 rpm for 15 min at 4 °C. Protamine sulfate at a final concentration of 0.1% w/v was added to the supernatant and stirred for 20-30 min, after which the solution was centrifuged 3 times at 14,000 rpm for 15 min at 4 °C. After the final spin, the supernatant was collected and incubated with Ni-NTA resin equilibrated in 20 mM Tris-HCl, pH 8.0, 350 mM NaCl, 1 mM ßME and 20 mM imidazole for 30 minutes at 4 °C. After incubation, the resin was washed with the same buffer until the A_{280} was 0.1 or less. The protein was subsequently eluted from the Ni-NTA column using 20 mM Tris-HCl, pH 8.0, 350 mM NaCl, 1mM ßME and 400 mM imidazole. The eluate was concentrated to ~5mg/mL (using ε_{280} = 1.18 mL mg^{-1}) and glycerol was added to a final concentration of 50% v/v. This final protein solution (2.5mg/mL) was flash frozen in small aliquots by immersion in liquid nitrogen and stored at −80 °C.

Generation of the lid deletion constructs

The gene for rat cPEPCK encoding the entire 622-residue protein was cloned into in the pSUMO expression plasmid using the methodology provide by the supplier (Lifesensors*).* This wild-type construct was used as the starting vector to create the lid deletion mutants (Ld_1g, Ld_2g, and Ld_3g). The forward primers (Ld_1g 5′-GCCATGAGATCAGAGGCATCATGCACGACCCCTTCGC-3′, Ld_2g 5′-GCCATGAGATCAGAGGGCGGTATCATGCACGACC-3’, and Ld_3g 5′-GCCATGAGATCAGAGGGCGGAGGTATCATGCACGACC -3′) and the respective reverse complement were utilized with the Stratagene Quik Change protocol. The resultant mutated DNA was isolated with a Hurricane cleanup kit from Gerard Biotech and sequenced in its entirety to confirm the presence of the desired mutation and the absence of any additional mutations introduced via the PCR protocol. The plasmid DNA was transformed into *E. Coli* BL-21(DE3) electro-competent cells for expression.

PEPCK expression and purification

Overnight cultures of BL-21(DE3) *E. coli* cells containing the SUMO-PEPCK plasmid (WT and mutants) were grown at 37 °C, 225 rpm in LB media supplemented with 50 μg/mL kanamycin. The cells were pelleted by centrifugation at 6000 rpm. The resultant cell pellet was resuspended and grown in 1.5L of LB-50 μg/mL kanamycin at 37 °C until the OD_{600} reached 1.0. The cells were subsequently induced with 1mM IPTG and grown for an additional 4h. The cells were harvested by centrifugation at 6000rpm for 15 min and then stored at −80 °C. The frozen pellet was resuspended in buffer A [25 mM HEPES, pH 7.5, 2

mM TCEP, 10% glycerol, 10 mM imidazole and 300 mM NaCl] and lysed by two passages through a French pressure cell. The cell debris was pelleted by centrifugation at 9000rpm for 15 min at 4 °C. Protamine sulfate at a final concentration of 0.1% w/v was added to the supernatant and stirred for 30 min, after which the solution was centrifuged 3 times at 14,000 rpm for 15min at 4 °C. After the final spin, the supernatant was collected and incubated with Ni-NTA resin for 30 min at 4 °C. After incubation, the resin was washed with buffer A until the A_{280} was 0.1 or less. The protein was subsequently eluted from the Ni-NTA with buffer B [25 mM HEPES, pH 7.5, 2 mM TCEP, and 300 mM imidazole]. The eluted protein was then incubated with 2.5 mg of recombinant SUMO protease for 1 h, concentrated to ~4 mL in a stirred-cell Amicon concentrator with a 30 kDa MW cutoff membrane. The concentrated solution was applied to a P6DG desalting column equilibrated in buffer C [25 mM HEPES, pH 7.5 and 2 mM TCEP] to remove the imidazole. The fractions containing protein were pooled and reincubated with the Ni-NTA resin (to remove the hydrolyzed SUMO tag, any uncleaved SUMO-PEPCK fusion and the his6-tagged SUMO protease) for 30 min and washed with buffer C till the A_{280} was 0.1 or less. PEPCK was subsequently collected in the flow through. The sample was then concentrated to ~15 mL and loaded onto a Hi-Q anion exchange column (BioRad) equilibrated in buffer D [25 mM HEPES, pH 7.5, 10 mM DTT] and eluted using a gradient of buffer D and buffer E [25 mM HEPES, pH 7.5, 10 mM DTT, 500 mM NaCl] using a BioRad Biologic FPLC system. The fractions containing the protein were pooled and concentrated in an Amicon concentrator to a final volume of 3 mL or less. The concentrated enzyme was subsequently loaded onto a P6DG desalting column equilibrated in buffer D to remove the NaCl. The fractions with an A280 above 0.3 were pooled and concentrated using a 30 kDa centricon concentrator to a final concentration of 10 mg/ml, determined by absorbance at A_{280} (ε_{280} = 1.7 mL mg^{-1}). The protein was then flash frozen by pipetting 30μL drops directly into liquid nitrogen and the protein pellets were stored at −80 °C.

Kinetic Experiments

PEPCK was assayed for enzymatic activity in the physiological direction of PEP formation and the reverse direction of OAA formation. In addition PEPCK was assayed for the spontaneous production of pyruvate during turnover and the decarboxylation of OAA to pyruvate in the presence of GDP. All assays were conducted as previously described (14) with the following alterations. The assay mixture for the decarboxylation and phosphorylation of OAA to form PEP contained 50 mM HEPES pH 7.5, 10 mM DTT, 5.8 mM $MgCl_2$, 450 μM GTP, 1mM ADP, 20 μM $MnCl_2$, 150 μM NADH, 30 units of LDH, 50 μg PK, and 350 μM OAA. The assay mixture for the dephosphorylation and carboxylation of PEP to form OAA was measured using 50 mM HEPES pH 7.5, 10 mM DTT, 17 mM $MgCl_2$, 20 μM $MnCl_2$, 4 mM GDP, 150 μM NADH, 5 mM PEP, 10 units of MDH, and 50 mM $KHCO_3$. The assay mixture for the spontaneous production of pyruvate during the OAA→PEP reaction was altered from that previously published by changing the concentrations of GTP, $MgCl_2$, and $MnCl_2$ used to 450 μM, 1.8 mM, and 20 μM, respectively. The assay mixture for the decarboxylation of OAA to form pyruvate in the presence of GDP was carried out with 4.2 mM GDP and 17 mM $MgCl_2$. The concentration of PEPCK utilized was 14-200 nM. For the estimation of the upper limits for the kinetic constants, the limit of detection for the continuous assay was determined to be 8×10^{-4} μmol min^{-1} mL^{-1}.

Nucleotide Binding

PEPCK's affinity for nucleotide was determined using intrinsic fluorescence quenching experiments as previously described (14) with the following alteration: the reaction mixture contained 50mM HEPES, pH 7.5, 10mM DTT, 1.4 mM $MgCl_2$, and PEPCK (1-5 μM).

Crystallization

Crystals of Ld_1g, Ld_2g, and Ld_3g PEPCK were grown by vapor diffusion using the hanging drop method. The well solution consisted of 22-26% PEG 3350, 100 mM HEPES pH 7.4, and water to obtain a final volume of 700 μL. All crystals except the Ld_2g-Mn^{2+}-PEP-Mn^{2+}GDP complex were grown on a siliconized cover slide in a liquid drop that contained 4μL of 10 mg/mL protein, 2μL of the well solution, 0.5μL of 30 mM GDP or GTP, and 0.5 μL of 75 mM $MnCl_2$. The crystals were cryoprotected and the corresponding complex formed by soaking the crystal for 30-60 min in a solution containing 25% PEG 3350, 10% PEG 400, 100 mM HEPES pH 7.4, 2 mM $MnCl_2$, 5 mM GDP or GTP, and 10 mM of either PEP, βSP or oxalate to generate the corresponding PEPCK-Mn^{2+}-βSP-Mn^{2+}GTP, PEPCK-Mn^{2+} PEP-Mn^{2+}GDP and PEPCK-Mn^{2+}-oxalate-Mn^{2+}GTP complexes. Crystals of the Ld_2g-Mn^{2+}-PEP-Mn^{2+}GDP complex were grown as above however the complex was obtained by co-crystallization in the presence of 30 mM GDP and 7 mM PEP. All crystals were cryo-cooled by immersion in liquid nitrogen.

Collection of diffraction data

Data on the cryo-cooled Ld_1g and Ld_3g PEPCK-Mn^{2+} βSP-Mn^{2+}GTP, Ld_1,2,3g PEPCK-Mn^{2+}-PEP Mn^{2+}GDP and Ld_1,2,3g PEPCK-Mn^{2+}-oxalate-Mn^{2+}GTP complexes maintained at 100K were collected at the Stanford Synchrotron Radiation Laboratory, Beamline 7-1, Menlo Park, CA. Data on the cryo-cooled Ld_2g PEPCK-Mn^{2+}-βSP-Mn^{2+}GTP complex maintained at 100K were collected on a Rigaku/MSC RU3HR rotating copper anode X-ray generator coupled to an R-AXIS IV++ detector with 2theta stage, Blue Osmic confocal mirrors and an XStream cryostat at the University of Kansas Medical Center. A summary of the data statistics is presented in Table 2.

Structure determination and refinement

The Ld_1,2,3g, mutant enzyme structures were solved by the molecular replacement method using MOLREP (23) in the CCP4 package (24) and the previously solved rat cPEPCK structures of the same complexes (PDB ID: 3DT4, 3DT7 and 3DTB) (11). For each complex, the molecular replacement solution was refined using Refmac5 followed by manual model adjustment and rebuilding using COOT (25). Ligand, metal, water addition and validation were also performed in COOT. Model validation, including Ramachandran statistics was performed using the Molprobity web server (http://molprobity.biochem.duke.edu) (26). A summary of the model statistics for all structures is presented in Table 2.

RESULTS AND DISCUSSION

Structural characterization of proteins via X-ray crystallography and NMR has led to the observation that enzymes and other proteins are inherently flexible molecules that can readily sample multiple low-energy conformations and that this conformational sampling is intrinsic to the protein's biological function (1, 27). One non-regular secondary structural element that has been observed in several enzyme systems to have mobile features that are critical to catalytic function is the Ω-loop (5, 7, 8, 10, 28-32). In several systems that have been characterized, this type of loop undergoes a transition from a catalytically inactive, open conformation to a catalytically active, closed conformation as the enzyme binds substrates (2, 3, 7, 9, 29, 33). In the case of PEPCK this open-closed transition of the Ω -loop is also accompanied by a disorder to order transition as the open Ω-loop is found to be conformationally dynamic, interconverting between two or more conformational states while upon closure the Ω–loop adapts a single conformational state. This ligand-gated transition has typically been identified by crystallographic analysis of differentially ligated enzyme complexes representing states along the enzyme catalyzed reaction coordinate (2, 4,

11). However, previous studies carried out on triosephosphate isomerase, glutathione synthetase, and ribulose-1,5-bisphosphate carboxylase/oxygenase illustrate that structural information on the WT enzyme alone does not reveal the entire role for an Ω-loop in catalysis (6-8).

Rational behind lid removal in PEPCK

Previously, it has been demonstrated that closure of the active site lid in PEPCK protected the reactive enolate intermediate formed during catalysis from spurious protonation and decoupling of the reaction through the formation of pyruvate(14). In addition, this work demonstrated that closure of the active site lid domain stabilizes the enolate intermediate resulting in catalytic rate enhancement. While this latter role was initially found to be surprising as stabilization of the intermediate is achieved without direct interaction between the lid domain and the substrates or intermediate there is precedence for this mechanism of stabilization. In the well-characterized Ω–loop of triosephosphate isomerase (TIM) the 'phosphate-gripper loop' functions to stabilize the enediolate intermediate of the reaction by 12 kcal mol^{-1} using only a single hydrogen bond between the backbone amide and the substrate phosphodianion (34). It has been suggested that a major contribution to catalytic function of the phosphate gripper loop in TIM is the result of a decrease in the effective dielectric constant upon loop closure that strengthens the substrate-enzyme interactions at the enzyme active site thereby accelerating catalysis (3). It is therefore reasonable to assume that the closure of the lid domain of PEPCK may have a similar impact upon the dielectric constant of the PEPCK active site, resulting in the tighter binding of the enolate intermediate upon lid closure. In order to further investigate the role of the active site lid in PEPCK function, we desired to excise the Ω-loop in its entirety from PEPCK. As previously mentioned, the unique architecture of an Ω-loop results in a narrow end-to-end distance between the location where the Ω-loop exits and re-enters the body of PEPCK. In the case of PEPCK this narrow distance results from the loop exiting and entering the structure on two adjacent strands of an antiparallel ß-sheet (strands 28 and 29) (Figure 1). This architecture results in the Cα of the loop hinge residues, A464 and V474, being, ~5 Å apart. We postulated that removing the 11-amino acid loop in PEPCK and replacing it with one, two, or three glycine residues would allow the loop to be removed with minimal distortion to the Ω-loop hinge regions and the overall fold of the protein. Upon expression and purification of these mutations (Ld_1g, Ld_2g, Ld_3g), we undertook structural and functional studies to ascertain the consequences of Ω-loop removal in order to build upon our understanding of the Ω-loop lid in PEPCK catalytic function.

Kinetic characterization of lid deletion constructs

Previous work on rat cPEPCK in the laboratory utilized a vector that fused cPEPCK to an N-terminal GST-tag assisting in expression of soluble enzyme and purification (11, 14, 35, 36). In that construct, after removal of the GST tag via digestion with thrombin, two non-native residues (glycine and serine) remained N-terminal to the native N-terminal methionine. For these studies, in order to obtain a more native protein, cPEPCK was cloned into a vector placing the enzyme C-terminal to a SUMO fusion. After cleavage of the SUMO tag using SUMO protease, the enzyme that is obtained begins at the native N-terminal methioinine residue. Characterization of this enzyme form when compared to the previous enzyme construct demonstrates little difference in the kinetic parameters ((14) and Table 1). In contrast, similar characterization of the three lid deletion mutants demonstrated that removal of the Ω-loop rendered all of the mutant enzymes incapable of catalyzing the interconversion of OAA and PEP (Table 1). Further supporting the lack of catalytic activity is the observation that the PEPCK-Mn^{2+}-PEP-Mn^{2+}GDP complex is stable to crystallization (see below, Figure 4) a feat that is not possible with the WT enzyme due to catalytic turnover. Based upon the lack of observable activity in the kinetic assays, an upper limit for

the activity of the mutant enzymes was calculated resulting in a reduction in k_{cat} of at least 10^6 (Table 1). This loss in PEPCK catalytic function is comparable to the reduction of k_{cat} by 5.3×10^4 observed upon truncation of the Ω –loop lid domain of triosephosphate isomerase (37). The inability of the lidless forms of PEPCK to catalyze the interconversion of OAA and PEP was not entirely unexpected. Previous work demonstrates that a key role of the lid is to protect the enolate intermediate from protonation and decoupling of the reaction to the formation of pyruvate (14). Therefore, *a priori* it was expected that the lidless enzymes would consume OAA and produce pyruvate rather than PEP. In contrast to this expectation the lidless enzymes in addition to being unable to catalyze the complete reaction, are also incapable of catalyzing the first half reaction, namely the decarboxylation of OAA (Scheme 1).

Structural characterization lidless PEPCK variants

The lack of any enzymatic activity in each of the kinetic assays for the Ld_1g, _2g, and _3g mutants demonstrates that lid removal equates to a complete loss of catalytic function. This raises the obvious question as to the source of the inactivity as the mobile Ω-loop contributes no catalytic residues to the chemical reaction. To investigate the source of the inactivity and illuminate additional roles for the Ω-loop in catalytic function, multiple crystallographic structures representing the Michaelis complexes for the forward and reverse reaction as well as the enolate intermediate complex were determined for each lidless enzyme variant as has been previously done for the WT enzyme (11). As mentioned above the only difference between these crystallographic complexes and the ones obtained previously for the WT enzyme was that due to the inactivity of the lid deletion constructs instead of using the PEP analogue, PGA, to obtain a complex representative of the PEP-GDP Michaelis-like complex, the authentic substrate PEP could be utilized to generate the authentic PEPCK-Mn^{2+}-PEP Mn^{2+}GDP complex. The crystallographic data illustrate that all the substrates still bind at reasonable concentrations to the active site of the lid-deletion constructs and with the exception of the Ld_1g and Ld_2g PEP-GDP complexes (discussed below) they form identical complexes to those observed in WT PEPCK (Figure 4). Therefore, the structural data demonstrate that the inactivity of the mutant enzyme forms is not due to an inability of the mutated enzymes to form the correct enzyme-substrate complexes and must be due to some other intrinsic requirement for the lid domain in the catalytic process.

Inspection of the structures demonstrates that the lid deletion mutants adapt an identical fold to WT PEPCK, which has been previously characterized as a unique kinase fold specific to PEPCK (4). At first glance, the structures of the lid deletion mutants are essentially indistinguishable from the open conformations of the same WT complexes with an overall Cα RMSD of ~0.49 Å. Similarly the three lidless enzymes are indistinguishable from one another with Cα RMSD values ranging between 0.29-0.34 Å. Upon closer inspection of the structures there are two regions where each mutant deviates from the WT and each other. These are the N-terminal region (residues 4-10) and the truncated Ω-loop region (460-474). The deviation at the N-terminal region is not unexpected as this region lacks secondary structure and is typically found in variable orientations in different crystallographic structures of cPEPCK (11, 14, 35, 36). The difference in the polypeptide backbone surrounding residues 460-474 is due to the variance in the number of glycines residues used to create the linker region between residues 460 and 474 (Figure 5). The highest degree of deviation is observed in the Ld_1g structure, which was expected due to the usage of a single glycine to make the turn between ß25 and ß26. With the addition of one and two glycine residues in the Ld_2g and Ld_3g constructs, the distortion in this region is lessened but still noticeable. Importantly, the distortion is localized to the positions at the ends of the two strands (> 15Å from the active site) and is not propagated further in the structure. These

results demonstrate that the lack of catalytic function is not to due to general, gross distortion of the three-dimensional structure of the enzyme in the lidless constructs.

Based upon the lack of gross structural distortion and the ability of the enzyme to bind and form the identical complexes to the WT enzyme we hypothesized that the removal of the active site lid domain alters the ability of PEPCK to transition between the conformational states that we have previously demonstrated are necessary for catalytic function (20). In the WT structures of the Michaelis-like complexes (PEPCK-ßSP-GTP/PEPCK-PEP(PGA)-GDP) complexes, there are two molecules in the asymmetric unit (ASU), with one molecule occupying a closed lid conformation and the other an open lid. The conformational changes that PEPCK must undergo in order for the closed lid conformation to be occupied have been previously detailed and demonstrate that the open form represents a substrate binding/product release competent form while the closed form of the enzyme is the catalytically competent form (11, 20). The lid deletion complexes demonstrate that the substrates/intermediate of the reaction bind in an identical fashion to the mutant constructs as they do to the lid-open form of the WT enzyme. However, without the lid present the enzymes fail to undergo the full transition from the substrate binding/product release form to the catalytically required chemically competent form (Figure 6). It has been previously determined that closure of enzyme is required for the correct positioning of the substrates at the active site, allowing for chemistry to occur. This transition impacts the phosphorylation half-reaction in two ways. Firstly, if the transition from the open to the closed state does not occur, PEP is positioned in outer-sphere coordination to the M1 metal ion and as a consequence is at too great a distance for direct in line phosphoryl transfer. Secondly, in the open form of the enzyme, the nucleotide binding pocket is elongated and as a consequence the nucleotide is shifted rearward in the binding pocket by ~1 1.5Å. This is the result of the enzyme failing to adapt a closed, catalytically competent conformation. While previous studies have focused upon the obvious closure of the Ω-loop lid domain when transitioning between the open and closed enzyme forms, transitioning of the enzyme from the open, substrate binding form, to the closed, chemically competent form not only involves closing of Ω-loop lid domain, but a general ‘clam-like’ closure of the N- and C-terminal lobes of PEPCK. In this ‘clam-like’ closure, the two lobes of the enzyme shift toward one another shortening the effective length of the nucleotide binding pocket and resulting in the nucleotide and its M2 metal moving closer to the M1 metal ion shortening the phosphoryl transfer distance (Figure 6). Coincident with this motion is the movement of the P-loop that cradles the ß and γ phosphates and moves along with the nucleotide upon the closure of the lobes and resultant shortening of the nucleotide-binding pocket. The structural data indicate despite the correct ligation of the enzyme that in the WT enzyme relieves structural constraints and allows the clam-like closure of the two lobes to occur, in the lidless enzymes there is only partial closure of the enzyme (Figure 6). This partial closure is not sufficient to allow for catalytic activity due to mispositioning of the substrates of the reaction resulting in a phosphoryl transfer distance that is too great in either reaction direction. The necessity for closure of the enzyme on the decarboxylation half-reaction has been demonstrated as both OAA and GDP are required to stimulate the decarboxylation of OAA in WT enzyme (38). The structural data support this work as they demonstrate that unlike the PEPCK-OAA complex the PEPCK-OAA GDP complex samples the closed conformation (36). Therefore, the data are all consistent with the inactivity of the lidless enzyme forms being due to the inability of these enzyme constructs to sample the fully closed conformation of the enzyme that is required for both phosphoryl transfer and decarboxylation/carboxylation.

Based upon the new evidence presented by this work as well as the past body of structural and functional work on PEPCK we propose that the closing of the active site Ω-loop lid domain, which originates and terminates in the C-terminal lobe of PEPCK, acts as a lever arm to mediate the N- and C-terminal lobe closure of the enzyme that is required for

catalysis. In this fashion, the closure of the Ω-loop lid domain brings the C-terminal lobe of the enzyme along with it as it adapts its closed conformation, reaching across the domain interface and covering the active site cleft (Figure 6). Further, it is likely that the lid domain also acts as a thermodynamic latch, stabilizing the lobe closed conformation through interactions between residues on the mobile loop (e.g. E469 and H470) and on the body of the enzyme (the R-loop) as it spans between the two domains. This would give the closed form of the enzyme a lifetime long enough to carry out the entire catalytic cycle without exposure of the enolate intermediate to solvent; an event that has been demonstrated to result in the decoupling of the reaction to pyruvate formation (14). If the later, thermodynamic latch function were the only function of the active site lid and the enzyme has an intrinsic propensity to open and close the N- and C-terminal lobes, we would expect to observe production of pyruvate by the lidless enzymes. This half reaction reactivity would be a result of the closure of the lobes stimulating decarboxylation as has been previously demonstrated (36, 38). Since this activity is not observed, the data are consistent with the proposed dual role for the lid domain.

In addition to the lack of the structural transition from the open to closed form of the enzyme, the structures of all three lid deletions constructs in the PEP-GDP complex demonstrate that lid removal results in alterations in the binding mode of GDP that in turn is correlated with a decreased/loss of binding of the M2 (nucleotide–associated) metal ion. (Figure 7). As is illustrated by the Ld_2g-PEP-GDP complex, this is the result of the P-loop remaining in its open state (depicted by the positions of S286 and T291 in Figure 7). This open P-loop conformation results in the GDP nucleotide shifting in the more open nucleotide-binding pocket (composed of residues 434-443 and 514-533, Figure 7) and a corresponding loss of M2 metal ion affinity as T291 coordinates to the beta-oxygen of the repositioned nucleotide rather than the M2 metal ion. In contrast the normal binding mode for GDP and the P-loop is observed in the Ld_3g complex, while a mixture of the two conformations is observed in the Ld_1g complex (Figure 7). In all structures the occupancy of the M2 metal ion is reduced suggesting a loss in its binding affinity due to the disorder in the nucleotide binding pocket resulting from the failure of the P-loop to adapt its more closed conformation.

Biochemical studies on PEPCK have shown that while the nucleotide will bind to the enzyme in the absence of the M2 metal ion, the enzyme has an absolute requirement for two divalent metal ions for enzymatic activity and the true substrate for the reaction is the M^{2+}-nucleotide complex (17-19). Previous structural studies on PEPCK support these biochemical studies and demonstrate that the first metal ion associates with the protein in the absence of any substrate acting as a true metal cofactor. The second metal ion is only observed when the di- or tri-phosphate is present with ligands contributed to its binding site by both the nucleotide phosphoryl oxygen atoms and the Oγ of T291 (4).

As discussed above, in lid deletion mutants in complex with GDP and PEP, the Mn^{2+} that is normally observed approximately 2.1 Å from the liganding oxygen atom is refined to a greatly reduced occupancy as the failure of the closure of the P-loop does not allow for correct coordination of the metal ion by the phosphate of GDP or the Oγ of T291. Support for the crystallographic data comes from fluorescence quenching experiments (Table 1) measuring nucleotide-binding affinity. These data demonstrate that consistent with the propensity for the P-loop to remain open in the presence of nucleotide and the resulting altered binding of nucleotide and the correspondingly decreased affinity for the binding of the M2 metal ion, the binding of the di- and tri-phosphate nucleotides is impacted when compared to the WT enzyme. The binding studies demonstrate that the largest change in ITP binding is observed with the Ld_1g construct which demonstrates ~5-fold effect (WT, 0.8 μM, Ld_1g, 4.7 μM). The largest change in the K_D for IDP is a 15-fold increase again this

maximal change is in the Ld_1g construct (WT IDP, 2.7μM, Ld_1g, 40 μM). These changes in the binding of nucleotide, while modest, are consistent with the loss of binding affinity for the M2 metal ion, an effect that is most apparent with the diphosphate nucleotide. In the absence of the γ-phosphate the binding of this the manganese ion is presumably weaker than the more highly ligated ion found in the presence of ITP/GTP (in the presence of the triphosphate nucleotide an oxygen atom from both the ß- and γ-phosphate coordinate to the M2 metal ion).

This shift in the ability of the enzyme to form the correctly liganded Mn^{2+}GDP complex would certainly decrease the ability of the enzymes to catalyze phosphoryl transfer step during the formation of OAA from PEP. However, it would not result in the complete lack of catalytic activity observed as the Ld_1g and Ld_3g lidless enzymes demonstrate that some population of the correct complex can form. Therefore, if the only defect imposed by lid removal were due to the alteration in GDP/manganese binding, we would observe partial overall activity and as mentioned previously, the enzymes would be active in the decarboxylation half reaction.

An additional unexpected observation in the Ld_1g structure was a minor conformation for the R-loop (amino acids 84-88), in which it is flipped out of the active site toward bulk solvent (Figure 8). Evidence for this alternate conformation is seen in all three oxalate-GTP complexes however the density is only suitable for modeling of the alternate state in the Ld_1g and Ld_3g complexes. Coupled with the departure of R87 from the active site pocket in this alternate coordination of the R-loop is a change in the metal coordination of the M1 metal ion. This is the result of K244 that typically acts as an M1 metal ligand, coordinating to the bound oxalate molecule replacing the ionic interaction lost by the displacement of R87 (Figure 8 inset). These structures of the lidless oxalate-GTP complexes represents the first time the R-loop has been observed in an alternative conformation. However, the isotropic B-factors of the R-loop in a series of crystal structures representing PEPCK transitioning along the reaction coordinate do suggest that this loop is a dynamic element of structure and undergoes an ordered (PEPCK, PEPCK-PEP, PEPCK-OAA) to disordered (PEPCK-GDP/GTP) to ordered (PEPCK-oxalate-GTP) transition, as the enzyme cycles through the catalytic reaction. This alternate conformation provides interesting insight into the coupling of loop motion and catalytic function in PEPCK. Previous structures demonstrate that the P-loop occupies an open conformation that sterically precludes lid closure in the absence of nucleotide binding. The question that remained was why the lid remained open until the second substrate (PEP or OAA) binds. The disorder in the R loop induced by nucleotide binding (36) and the alternate conformation of the R-loop illustrated in these lidless enzymes suggest that it is the mobility induced into the R-loop upon formation of the PEPCK-nucleotide complexes that prevents Ω-loop closure in the absence of OAA/PEP. The subsequent binding of OAA/PEP and the interaction of the R-loop with PEP/OAA via R87 stabilizes the R-loop and allows the lid to sample the closed, catalytically active conformation and move to generation of the enolate. This mobility of R87 and the R-loop in which it resides, and the prevention of the transition of PEPCK from the open to closed state also provide an explanation as to why PEPCK is not observed to function as a GTPase.

As demonstrated in these studies as well as work on other well characterized enzymes such as TIM and orotidine 5′-monophosphate decarboxylase the coupling between catalytic function and the ability of an enzyme to transition between open and closed conformational states is quite prevalent (3, 12, 33). The work presented here further demonstrates how an enzyme's catalytic function can be abolished through the loss of the ability of an enzyme to adapt a conformation that is required for function despite all active site elements required for chemical conversion of substrates into products remaining intact. More broadly, these

studies highlight the potential pitfalls associated with the common practice of inferring the functional importance of regions of protein structure without careful structural and functional characterization.

Acknowledgments

The authors would like to thank Sarah Sullivan for providing the data on the inhibition of PEPCK by oxalate.

Funding Sources T.H. acknowledges support from National Center for Research Resources P20 RR17708 and the Natural Sciences and Engineering Research Council of Canada.

Portions of this research were carried out at the Stanford Synchrotron Radiation Laboratory, a national user facility operated by Stanford University on behalf of the U.S. Department of Energy, Office of Basic Energy Sciences. The SSRL Structural Molecular Biology Program is supported by the Department of Energy, Office of Biological and Environmental Research, and by the National Institutes of Health, National Center for Research Resources, Biomedical Technology Program, and the National Institute of General Medical Sciences.

REFERENCES

1. Ma B, Nussinov R. Enzyme dynamics point to stepwise conformational selection in catalysis. Current Opinion in Chemical Biology. 2010; 14:652–659. [PubMed: 20822947]
2. Fetrow J. Omega loops: nonregular secondary structures significant in protein function and stability. The FASEB Journal. 1995; 9:708–717.
3. Malabanan MM, Amyes TL, Richard JP. A role for flexible loops in enzyme catalysis. Current Opinion in Structural Biology. 2010; 20:702–710. [PubMed: 20951028]
4. Holyoak T, Sullivan SM, Nowak T. Structural Insights into the Mechanism of PEPCK Catalysis. Biochemistry. 2006; 45:8254–8263. [PubMed: 16819824]
5. Banerjee S, Pieper U, Kapadia G, Pannell LK, Herzberg O. Role of the Ω-Loop in the Activity, Substrate Specificity, and Structure of Class A β-Lactamase†,‡. Biochemistry. 1998; 37:3286–3296. [PubMed: 9521648]
6. Pompliano DL, Peyman A, Knowles JR. Stabilization of a reaction intermediate as a catalytic device: definition of the functional role of the flexible loop in triosephosphate isomerase. Biochemistry. 1990; 29:3186–3194. [PubMed: 2185832]
7. Kato H, Tanaka T, Yamaguchi H, Hara T, Nishioka T, Katsube Y, Oda J. i. Flexible Loop That Is Novel Catalytic Machinery in a Ligase. Atomic Structure and Function of the Loopless Glutathione Synthetase. Biochemistry. 1994; 33:4995–4999. [PubMed: 8172874]
8. Larson EM, Larimer FW, Hartman FC. Mechanistic insights provided by deletion of a flexible loop at the active site of ribulose-1,5-bisphosphate carboxylase/oxygenase. Biochemistry. 1995; 34:4531–4537. [PubMed: 7718555]
9. Sampson NS, Kass IJ, Ghoshroy KB. Assessment of the Role of an Ω Loop of Cholesterol Oxidase: A Truncated Loop Mutant Has Altered Substrate Specificity†. Biochemistry. 1998; 37:5770–5778. [PubMed: 9548964]
10. Kempf JG, Jung JY, Ragain C, Sampson NS, Loria JP. Dynamic requirements for a functional protein hinge. J Mol Biol. 2007; 368:131–149. [PubMed: 17336327]
11. Sullivan SM, Holyoak T. Enzymes with lid-gated active sites must operate by an induced fit mechanism instead of conformational selection. Proc Natl Acad Sci U S A. 2008; 105:13829–13834. [PubMed: 18772387]
12. Malabanan MM, Amyes TL, Richard JP. Mechanism for Activation of Triosephosphate Isomerase by Phosphite Dianion: The Role of a Ligand-Driven Conformational Change. Journal of the American Chemical Society. 2011; 133:16428–16431. [PubMed: 21939233]
13. Sullivan SM, Holyoak T. Structures of rat cytosolic PEPCK: insight into the mechanism of phosphorylation and decarboxylation of oxaloacetic acid. Biochemistry. 2007; 46:10078–10088. [PubMed: 17685635]
14. Johnson TA, Holyoak T. Increasing the conformational entropy of the Omega-loop lid domain in phosphoenolpyruvate carboxykinase impairs catalysis and decreases catalytic fidelity. Biochemistry. 2010; 49:5176–5187. [PubMed: 20476774]

15. McNicholas S, Potterton E, Wilson KS, Noble MEM. Presenting your structures: the CCP4mg molecular graphics software. Acta Crystallographica Section D-Biological Crystallography. 2011; 67:386–394.
16. Yang J, Kalhan SC, Hanson RW. What is the metabolic role of phosphoenolpyruvate carboxykinase? J Biol Chem. 2009; 284:27025–27029. [PubMed: 19636077]
17. Colombo G, Carlson GM, Lardy HA. Phosphoenolpyruvate carboxykinase (guanosine 5′-triphosphate) from rat liver cytosol. Dual-cation requirement for the carboxylation reaction. Biochemistry. 1981; 20:2749–2757. [PubMed: 6788070]
18. Lee MH, Hebda CA, Nowak T. The role of cations in avian liver phosphoenolpyruvate carboxykinase catalysis. Activation and regulation. J Biol Chem. 1981; 256:12793–12801. [PubMed: 6796577]
19. Hebda CA, Nowak T. Phosphoenolpyruvate carboxykinase. Mn2+ and Mn2+ substrate complexes. J Biol Chem. 1982; 257:5515–5522. [PubMed: 7068604]
20. Carlson GM, Holyoak T. Structural insights into the mechanism of phosphoenolpyruvate carboxykinase catalysis. J Biol Chem. 2009; 284:27037–27041. [PubMed: 19638345]
21. Tari LW, Matte A, Pugazhenthi U, Goldie H, Delbaere LT. Snapshot of an enzyme reaction intermediate in the structure of the ATP-Mg2+-oxalate ternary complex of Escherichia coli PEP carboxykinase. Nat Struct Biol. 1996; 3:355–363. [PubMed: 8599762]
22. Griffith OW, Weinstein CL. beta-Sulfopyruvate. Methods Enzymol. 1987; 143:221–223. [PubMed: 3657538]
23. Vagin A, Teplyakov A. MOLREP: an Automated Program for Molecular Replacement. Journal of Applied Crystallography. 1997; 30:1022–1025.
24. Collaborative. The CCP4 suite: programs for protein crystallography. Acta Crystallographica Section D. 1994; 50:760–763.
25. Emsley P, Lohkamp B, Scott WG, Cowtan K. Features and development of Coot. Acta Crystallogr D Biol Crystallogr. 2010; 66:486–501. [PubMed: 20383002]
26. Chen VB, Arendall WB 3rd, Headd JJ, Keedy DA, Immormino RM, Kapral GJ, Murray LW, Richardson JS, Richardson DC. MolProbity: all-atom structure validation for macromolecular crystallography. Acta Crystallogr D Biol Crystallogr. 2010; 66:12–21. [PubMed: 20057044]
27. Henzler-Wildman KA, Thai V, Lei M, Ott M, Wolf-Watz M, Fenn T, Pozharski E, Wilson MA, Petsko GA, Karplus M, Hubner CG, Kern D. Intrinsic motions along an enzymatic reaction trajectory. Nature. 2007; 450:838–844. [PubMed: 18026086]
28. Williams JC, McDermott AE. Dynamics of the flexible loop of triosephosphate isomerase: the loop motion is not ligand gated. Biochemistry. 1995; 34:8309–8319. [PubMed: 7599123]
29. Xiang J, Jung J. -y. Sampson NS. Entropy Effects on Protein Hinges: The Reaction Catalyzed by Triosephosphate Isomerase†. Biochemistry. 2004; 43:11436–11445. [PubMed: 15350130]
30. Johnson TA, Qiu J, Plaut AG, Holyoak T. Active-Site Gating Regulates Substrate Selectivity in a Chymotrypsin-Like Serine Protease The Structure of Haemophilus influenzae Immunoglobulin A1 Protease. J Mol Biol. 2009
31. Sampson NS, Knowles JR. Segmental motion in catalysis: investigation of a hydrogen bond critical for loop closure in the reaction of triosephosphate isomerase. Biochemistry. 1992; 31:8488–8494. [PubMed: 1390633]
32. Sampson NS, Knowles JR. Segmental movement: definition of the structural requirements for loop closure in catalysis by triosephosphate isomerase. Biochemistry. 1992; 31:8482–8487. [PubMed: 1390632]
33. Desai BJ, Wood BM, Fedorov AA, Fedorov EV, Goryanova B, Amyes TL, Richard JP, Almo SC, Gerlt JA. Conformational Changes in Orotidine 5′-Monophosphate Decarboxylase: A Structure-Based Explanation for How the 5−-Phosphate Group Activates the Enzyme. Biochemistry. 2012
34. Amyes TL, O'Donoghue AC, Richard JP. Contribution of phosphate intrinsic binding energy to the enzymatic rate acceleration for triosephosphate isomerase. J Am Chem Soc. 2001; 123:11325–11326. [PubMed: 11697989]
35. Stiffin R,M, Sullivan SM, Carlson GM, Holyoak T. Differential inhibition of cytosolic PEPCK by substrate analogues. Kinetic and structural characterization of inhibitor recognition. Biochemistry. 2008; 47:2099–2109. [PubMed: 18197707]

36. Sullivan SM, Holyoak T. Structures of rat cytosolic PEPCK: Insight into the mechanism of phosphorylation and decarboxylation of oxaloacetic acid. Biochemistry. 2007; 46:10078–10088. [PubMed: 17685635]

37. Pompliano DL, Peyman A, Knowles JR. Stabilization of a reaction intermediate as a catalytic device: definition of the functional role of the flexible loop in triosephosphate isomerase. Biochemistry. 1990; 29:3186–3194. [PubMed: 2185832]

38. Noce PS, Utter MF. Decarboxylation of oxalacetate to pyruvate by purified avian liver phosphoenolpyruvate carboxykinase. J Biol Chem. 1975; 250:9099–9105. [PubMed: 392]

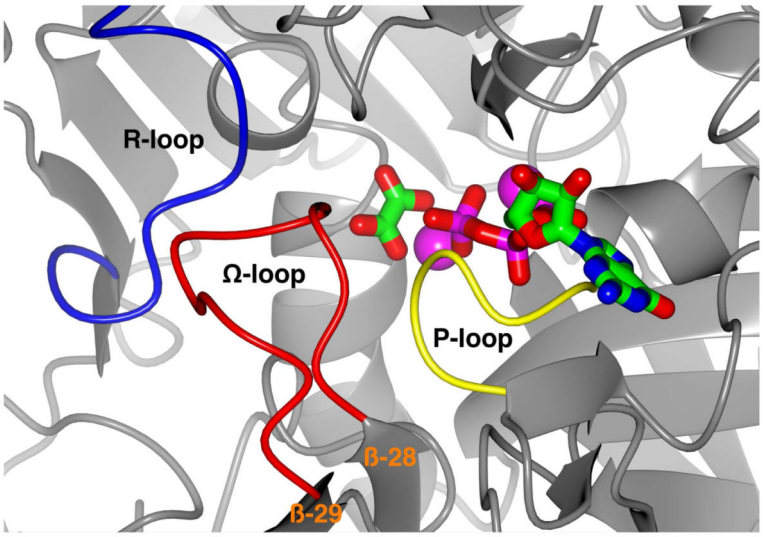

Figure 1.
The active site loops of cPEPCK. The catalytically important mobile loop elements at the active site of PEPCK, the R-loop (85-92), the P-loop (284-292) and the Ω-loop lid (464-474) are labeled and colored blue, yellow and red, respectively. Oxalate and GTP are rendered as stick models and colored by atom type. The M1 and M2 manganese ions are colored as pink spheres. All graphics were generated using CCP4MG (15).

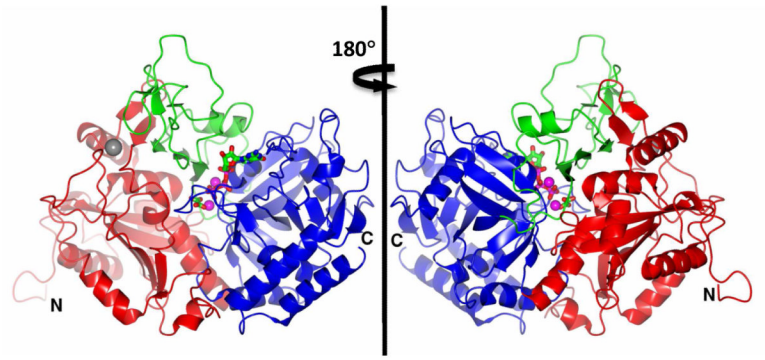

Figure 2.

The domain structure of cPEPCK. The N-terminal lobe (residues 1-259), the nucleotide binding domain (residues 260-325 and 426-622), and the PEPCK-specific domain (residues 326-425), are rendered in red, blue and green, respectively. The molecule on the right is related to the molecule on the left by a rotation of 180° about the vertical axis illustrated. Oxalate and GTP are rendered as stick molecules colored by atom type and the manganese ions are rendered as pink spheres to illustrate the location of the bound substrates and the active site. The N- and C-termini are also labeled.

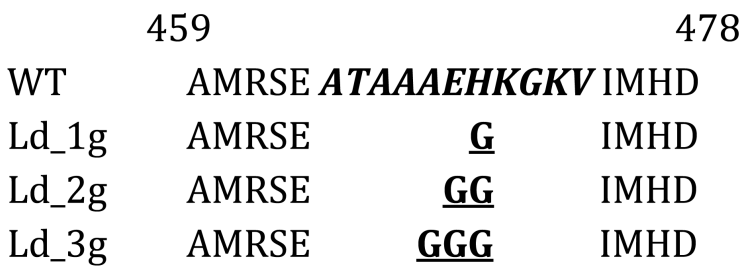

Figure 3.
The amino acid sequence in the region of the PEPCK Ω-loop lid for WT and Ld_1g, _2g, and _3g PEPCK. The residues used to replace the Ω-loop in the deletion constructs are rendered in bold and underlined. The sequence of the WT Ω-loop lid is italicized and rendered in bold.

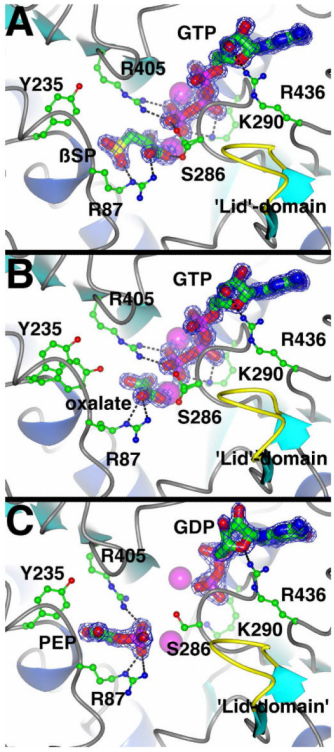

Figure 4.

Active site regions of Ld _3g lidless PEPCK The A) PEPCK-βSP—Mn^{2+}—Mn^{2+}GTP , B) oxalate— Mn^{2+}—Mn^{2+}GTP, and the C)PEP— Mn^{2+}—GDP complexes are illustrated. The active site residues are rendered as ball-and-stick models, the ligands are modeled as cylinders, and both are colored by atom type. The M1 and M2 Mn^{2+} ions are shown as pink spheres. The truncated Ω-loop lid is colored yellow. Dashed lines represent side chain-ligand interactions. 2Fo-Fc density for the ligands is shown as a blue mesh rendered at 1.5 σ. The dashed lines represent potential ligand-protein interactions.

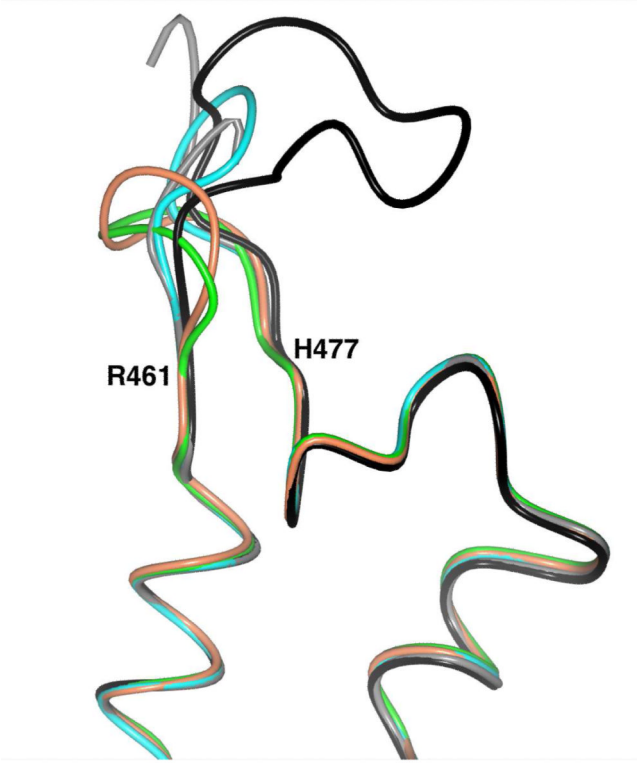

Figure 5.
Superposing of the Ω-loop lid regions of lidless PEPCK. The region of the structures corresponding to residues 450-496 is illustrated for the Ld_1g (green), Ld_2g (orange), Lg_3g (cyan), WT_open (grey) and WT_closed (black) PEPCK-Mn^{2+}-ßSP-Mn^{2+}GTP complexes. The residues R461 and H477 are labeled for reference.

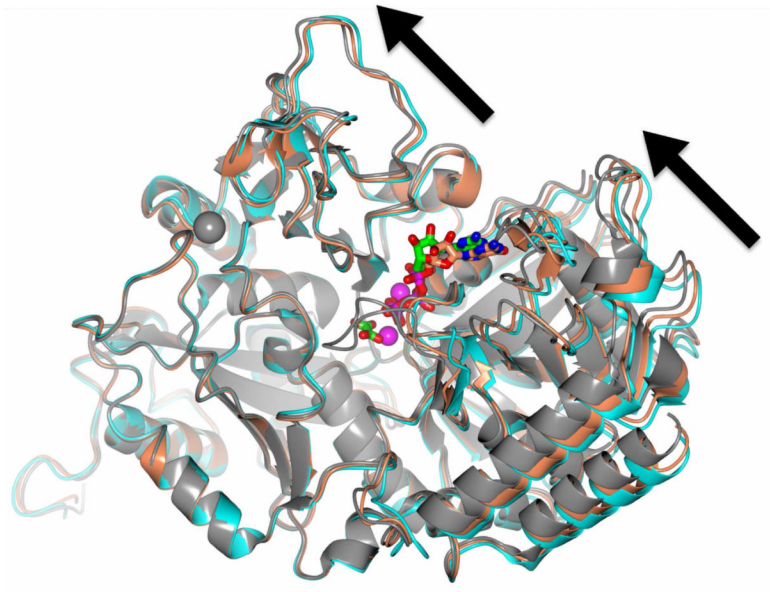

Figure 6.

Superposing of the open and closed enzyme forms of WT PEPCK and Ld_3g lidless PEPCK. The WT open (PGA-GDP, cyan) complex, the WT closed oxalate-GDP complex (gray), and Ld_3g lidless PEPCK in the oxalate-GTP complex (tan) are illustrated. The bound nucleotide in the WT-PGA-GDP complex is colored by atom type with tan carbons and the nucleotide in the closed WT-oxalate-GTP complex is colored by atom type with green carbons. This representation illustrates the impact of enzyme closure upon the position of the bound nucleotide. The large arrows illustrate the displacement in the C-terminal and PEPCK-specific domains progressing from the fully open, PGA-GDP complex, through the partially closed Ld_3g-oxalate-GTP complex, to the fully closed WT-oxalate-GTP complex. The orientation of the enzyme in this composite figure is the same as in Figure 2.

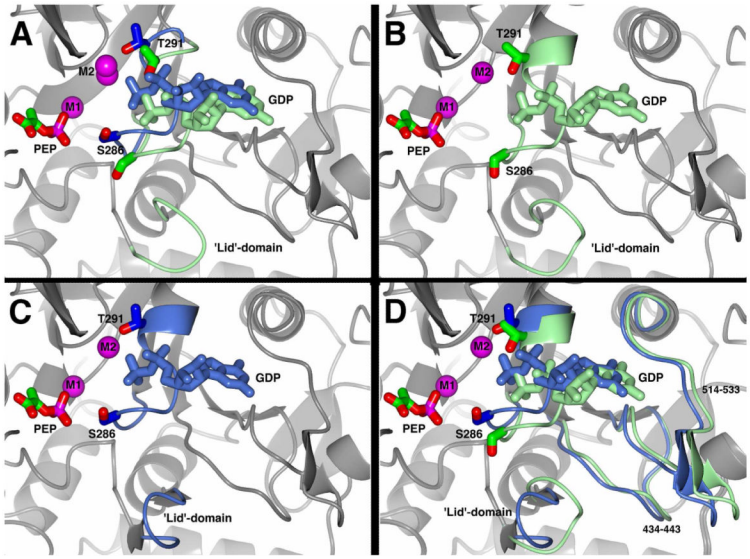

Figure 7.

Alterations to the binding mode of GDP in the lidless A) Ld_1g, B) Ld_2g and C) Ld_3g PEPCK-Mn^{2+}-PEP-Mn^{2+}GDP complexes. The protein and nucleotide conformations corresponding to the normal position of GDP found in the WT PEPCK-Mn^{2+}-PEP-Mn^{2+}GDP complex are rendered in light blue. The protein and nucleotide conformation corresponding to the abnormal position of GDP found in the Ld_1g and Ld_2g-Mn^{2+}-PEP-Mn^{2+}GDP complexes are rendered in light green. In D) a superpositioning of the Ld_2g and Ld_3g complexes (panels B and C) is shown illustrating the changes in the position of the P-loop (delineated by S286 and T291) and the nucleotide binding pocket (234-443, 514-533) corresponding to the two modes of GDP binding.

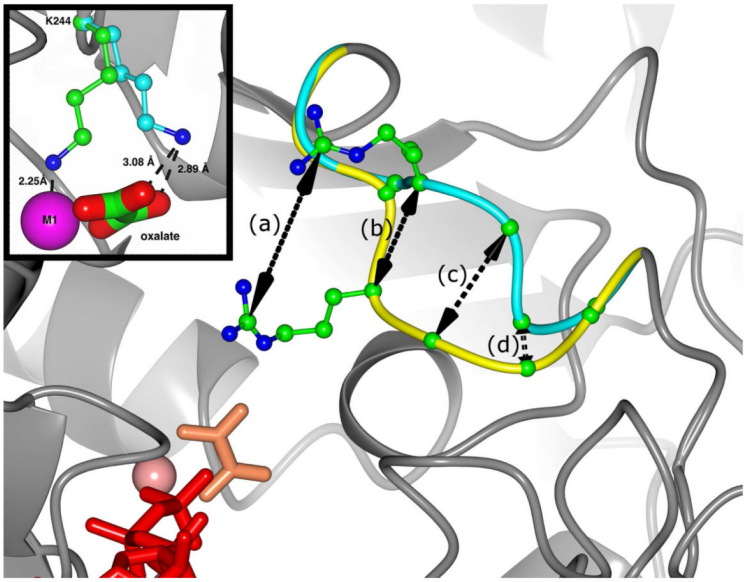

Figure 8.

The alternate conformation for the R-loop observed in the Ld_1g-oxalate-Mn^{2+}-Mn^{2+}GTP complex. The two conformations of the R-loop are shown in yellow (typical) and cyan (alternate conformation). Arginine 87 is rendered as a ball and stick model exhibiting a maximal displacement of 9.9Å at CZ (a). The other distances depicted are an ~6Å displacement at Cα of R87 (b) and the movement of Cα of residues A86(c) and V85 (d) by 5.5Å and 1.8Å, respectively. GTP (red), oxalate (tan) and the M1 manganese ion (pink) illustrate the location of the bound substrates and the position of the active site. Inset: the effect of R87 departure upon M1 metal ion coordination and oxalate interactions. Upon the movement of R87 out of the active site, K244 (green) moves from being a ligand to the M1 manganese ion to stabilizing the negative charge on oxalate (cyan). The coordination shell of the M1 manganese (pink) is filled upon departure of K244 by a water molecule (not shown).

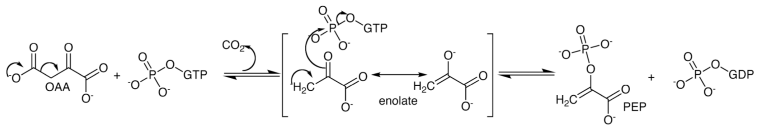

Scheme 1.
The reaction catalyzed by PEPCK.

Table 1

Characterization of wild-type and lidless PEPCKs. All experiments were performed at 25°C.

(A) OAA + GTP → PEP + GDP + CO_2					
Enzyme	**K_M (μM)**		**k_{cat} (s^{-1})**	**k_{cat}/K_M (M^{-1} s^{-1})**	
	OAA	**GTP**		**OAA**	**GTP**
Wild-type	51 ± 4	55 ± 5	52 ± 1	1.0×10^6	9.5×10^5
Ld_1g	ND	ND	$<1.4 \times 10^{-5}$	<0.3	<0.3
Ld_2g	ND	ND	$<1.4 \times 10^{-5}$	<0.3	<0.3
Ld_3g	ND	ND	$<1.4 \times 10^{-5}$	<0.3	<0.3

(B) PEP + CO_2 + GDP → OAA + GTP							
Enzyme	**K_M (μM)**			**k_{cat} (s^{-1})**	**k_{cat}/K_M (M^{-1} s^{-1})**		
	PEP	**GDP**	**CO_2**		**PEP**	**GDP**	**CO_2**
Wild-type	475 ± 14	207 ± 23	4000 ± 400	19 ± 1	3.7×10^4	9.2×10^4	4.6×10^3
Ld_1g	ND	ND	ND	$<1.4 \times 10^{-5}$	$<2.9 \times 10^{-2}$	$<6.8 \times 10^{-2}$	$<3.5 \times 10^{-3}$
Ld_2g	ND	ND	ND	$<1.4 \times 10^{-5}$	$<2.9 \times 10^{-2}$	$<6.8 \times 10^{-2}$	$<3.5 \times 10^{-3}$
Ld_3g	ND	ND	ND	$<1.4 \times 10^{-5}$	$<2.9 \times 10^{-2}$	$<6.8 \times 10^{-2}$	$<3.5 \times 10^{-3}$

(C) Decarboxylation Half-Reaction; OAA + GDP → Pyruvate + GDP + CO_2			
Enzyme	**K_M (μM)**	**k_{cat} (s^{-1})**	**k_{cat}/K_M (M^{-1} s^{-1})**
	OAA		
Wild-type	404 ± 28	2.0 ± 0.1	5.0×10^3
Ld_1g	ND	$<1.4 \times 10^{-5}$	$<3.4 \times 10^{-2}$
Ld_2g	ND	$<1.4 \times 10^{-5}$	$<3.4 \times 10^{-2}$
Ld_3g	ND	$<1.4 \times 10^{-5}$	$<3.4 \times 10^{-2}$

(D) Substrate/Substrate Analogue Affinities					
Enzyme	**K_D (μM)**	**K_D (μM)**	**K_I (μM)**	**K_I (μM)**	**K_I (μM)**
	ITP	**IDP**	**ßSP**	**PGA**	**oxalate**
Wild-type	0.8 ± 0.1	2.7 ± 0.1	25 ± 6	2530 ± 13	9 ± 1 *(a)* / 106 ± 6 *(b)*
Ld_1g	4.7 ± 0.3	40 ± 4	ND	ND	ND
Ld_2g	2.4 ± 0.3	16 ± 2	ND	ND	ND
Ld_3g	3.2 ± 0.3	32 ± 3	ND	ND	ND

ND; not determined due to inactivity of enzyme.

(a) measured against OAA.

(b) measured against PEP (11).

Table 2

Crystallographic data and model statistics for the PEPCK-Mn^{2+}-ßSP-Mn^{2+}GTP, PEPCK-Mn^{2+}-PEP-Mn^{2+}GDP and PEPCK-Mn^{2+}-oxalate-Mn^{2+}GTP complexes of Ld_1g, Ld_2g and Ld_3g PEPCK[a].

	Ld_1g PEPCK–Mn^{2+}–βSP–Mn^{2+}GTP	**Ld_1g PEPCK–Mn^{2+}–PEP–GDP**	**Ld_1g PEPCK–Mn^{2+}–oxalate–Mn^{2+}GTP**	**Ld_2g PEPCK–Mn^{2+}–βSP–Mn2+GTP**	**Ld_2g PEPCK–Mn^{2+}–PEP–GDP**	**Ld_2g PEPCK–Mn^{2+}–oxalate–Mn^{2+}GTP**	**Ld_3g PEPCK–Mn^{2+}–βSP–Mn^{2+}GTP**	**Ld_3g PEPCK–Mn^{2+}–PEP–+GDP**	**Ld_3g PEPCK–Mn^{2+}–oxalate–Mn^{2+}GTP**
PDB ID	**4GMM**	**4GMW**	**4GMU**	**4GMZ**	**4GNL**	**4GNM**	**4GNO**	**4GNP**	**4GNQ**
X-ray source	**SSRL Beamline 7-1**	**SSRL Beamline 7-1**	**SSRL Beamline 7-1**	**KUMC rotating anode**	**SSRL Beamline 7-1**	**SSRL Beamline 7-1**	**SSRL Beamline 7-1**	**SSRL Beamline 7-1**	**SSRL Beamline 7-1**
wavelength (Å)	0.9	0.9	0.9	1.54	1.15	0.9	0.9	0.9	0.9
space group	$P2_12_12_1$	$P2_12_12_1$	$P2_12_12_1$	$P2_12_12_1$	$P2_12_12_1$	$P2_12_12_1$	$P2_12_12_1$	$P2_12_12_1$	$P2_12_12_1$
unit cell	a = 60.6 Å	a = 61.1 Å	a = 60.5 Å	a = 60.6 Å	a = 61.3 Å	a = 60.5 Å	a = 60.8 Å	a = 60.9 Å	a = 60.5 Å
	b = 85.4 Å	b = 84.9 Å	b = 85.5 Å	b = 83.9 Å	b = 84.8 Å	b = 84.7 Å	b = 84.1 Å	b = 84.6 Å	b = 84.3 Å
	c = 118.9 Å	c = 119.3 Å	c = 118.8 Å	c = 118.6 Å	c = 119.0 Å	c = 118.8 Å	c = 118.6 Å	c = 118.8 Å	c = 119.0 Å
	α = β = γ 90 °	α = β = γ 90 °	α = β = γ 90 °	α = β = γ 90 °	α = β = γ 90 °	α = β = γ 90 °	α = β = γ 90 °	α = β = γ 90 °	α = β = γ 90 °
resolution limits, (Å)	39.4-1.74	33.3-1.75	27.0-1.20	30.8-2.05	34.9-1.70	26.7-1.50	34.3-1.50	34.7-1.74	27.4-1.40
no. of unique reflections	62571	62471	188021	37090	68183	94980	91864	61576	119287
completeness, % (highest resolution bin)	98.6 (96.0)	97.9 (94.5)	97.9 (94.0)	95.8 (73.6)	99.9 (100)	96.3 (96.5)	93.8 (86.4)	97.6 (98.9)	98.6 (90.2)
redundancy	3.8 (3.7)	4.5 (4.3)	3.9 (3.2)	11.7 (5.5)	8.7 (7.1)	4.4 (4.2)	4.5 (4.4)	5.0 (4.5)	8.4 (5.3)
$I/\sigma_{(I)}$	14.0 (2.0)	16.2 (2.1)	25.0 (2.7)	15.8 (2.1)	27.0 (2.0)	9.0 (1.5)	19.8 (2.5)	18.2 (2.5)	28.4 (1.5)
R_{merge}	0.07 (0.56)	0.08 (0.54)	0.03 (0.29)	0.09 (0.48)	0.06 (0.83)	0.12 (0.61)	0.044 (0.44)	0.044 (0.40)	0.045 (0.64)
no. of ASU molecules	1	1	1	1	1	1	1	1	1
R_{free}	22.4 (36.0	25.9 (33.7	19.6 (25.7	23.2 (34.0	23.3 (34.8	22.2 (38.0	19.4 (26.1	24.0 (29.6	19.7 (39.2)
R_{work}	18.9 (31.3	21.0 (30.0	17.1 (25.5	18.6 (26.0	19.4 (28.2	19.0 (36.7	16.9 (25.2	18.7 (27.5	17.5 (35.1)
average B values									

	Ld_1g PEPCK–Mn^{2+}–βSP–Mn^{2+}GTP	**Ld_1g PEPCK–Mn^{2+}–PEP–GDP**	**Ld_1g PEPCK–Mn^{2+}–oxalate–Mn^{2+}GTP**	**Ld_2g PEPCK–Mn^{2+}–βSP–Mn2+GTP**	**Ld_2g PEPCK–Mn^{2+}–PEP–GDP**	**Ld_2g PEPCK–Mn^{2+}–oxalate–Mn^{2+}GTP**	**Ld_3g PEPCK–Mn^{2+}–βSP–Mn^{2+}GTP**	**Ld_3g PEPCK–Mn^{2+}–PEP–+GDP**	**Ld_3g PEPCK–Mn^{2+}–oxalate–Mn^{2+}GTP**
PDB ID	**4GMM**	**4GMW**	**4GMU**	**4GMZ**	**4GNL**	**4GNM**	**4GNO**	**4GNP**	**4GNQ**
X-ray source	**SSRL Beamline 7-1**	**SSRL Beamline 7-1**	**SSRL Beamline 7-1**	**KUMC rotating anode**	**SSRL Beamline 7-1**	**SSRL Beamline 7-1**	**SSRL Beamline 7-1**	**SSRL Beamline 7-1**	**SSRL Beamline 7-1**
protein	29.98	30.07	14.31	25.20	30.39	25.97	16.80	25.00	17.98
water	36.18	35.61	27.46	32.80	36.01	36.59	29.06	35.29	30.31
ßSP	19.67	NA	NA	16.15	NA	NA	11.07	NA	NA
oxalate	NA	NA	11.99	NA	NA	21.50	NA	NA	13.48
PEP	NA	21.23	NA	NA	24.52	NA	NA	18.37	NA
GDP	NA	27.82	NA	NA	36.44	NA	NA	25.34	NA
GTP	22.88	NA	9.81	18.21	NA	21.16	10.65	NA	12.11
Mn^{2+}	21.01	34.9	7.71	21.89	23.49	17.30	9.34	23.74	9.48
Na^{+}	32.38	30.45	13.00	43.37	37.77	23.53	23.95	25.33	19.45
estimated coordinate error based on maximum likelihood (Å)	0.09	0.10	0.03	0.13	0.08	0.07	0.05	0.09	0.04
bond length rmsd (Å)	0.013	0.012	0.021	0.006	0.012	0.014	0.012	0.012	0.017
bond angle rmsd (deg)	1.63	1.66	2.06	1.15	1.53	1.67	1.59	1.54	1.91
Ramachandran Statistics (favored, outliers) (%)	97.2, 0	97.2, 0	97.2, 0	95.8, 0	96.7, 0	97.5, 0	97.6, 0.2	96.7, 0.3	97.4, 0.3

[a]Data in parentheses represent the data for the highest resolution shell. NA, not applicable.